

# Sequential Regeneration of Charmonia in Heavy-Ion Collisions

Xiaojian Du and Ralf Rapp

*Cyclotron Institute and Department of Physics and Astronomy,  
Texas A&M University, College Station, TX 77843-3366, USA*

(Dated: June 10, 2019)

We investigate the production of  $\psi(2S)$  in nuclear collisions at RHIC and LHC energies. We first address charmonium production in 200 GeV d-Au collisions at RHIC; the strong suppression of  $\psi'$  mesons observed in these reactions indicates mechanisms beyond initial cold nuclear matter effects. We find that a more complete treatment of hadronic dissociation reactions leads to appreciable  $\psi'$  suppression in the hadronic medium of an expanding fireball background for d-Au collisions. When implementing the updated hadronic reaction rates into a fireball for 2.76 TeV Pb-Pb collisions at LHC, the regeneration of  $\psi'$  mesons occurs significantly later than for  $J/\psi$ 's. Despite a smaller total number of regenerated  $\psi'$ , the stronger radial flow at their time of production induces a marked enhancement of their  $R_{AA}$  relative to  $J/\psi$ 's in a momentum range  $p_t \simeq 3$ -6 GeV. We explore the consequences and uncertainties of this “sequential regeneration” mechanism on the  $R_{AA}$  double ratio and find that it can reproduce the trends observed in recent CMS data.

PACS numbers:

## I. INTRODUCTION

Charmonium production in ultra-relativistic heavy-ion collisions (URHICs) has been studied for over 30 years. The originally proposed  $J/\psi$  suppression signature of Quark-Gluon Plasma (QGP) formation [1] has evolved into a more complex problem where both suppression and so-called regeneration (or statistical hadronization) mechanisms need to be considered. Their interplay and relevance depend on collision energy, system size and the 3-momentum of the measured charmonia, see, e.g., Refs. [2–4] for recent reviews. The phenomenological modeling of these mechanisms, and their relation to the underlying in-medium properties, has progressed significantly in recent years. In particular, kinetic transport approaches, when calibrated with existing data from SPS and RHIC, have shown predictive power in describing novel features of the  $J/\psi$  production systematics observed in the new energy regime of the LHC [5–8] (although significant uncertainties due to, e.g., the open-charm cross section persist [9]). This includes the marked increase of the nuclear suppression factor compared to RHIC energies, along with its pronounced dependence in transverse momentum.

Much less is known about the  $2S$  excited state,  $\psi'(3686)$ . Its small “binding” energy of about 45 MeV (relative to the  $D\bar{D}$  threshold) renders controlled theoretical calculations of its in-medium properties (binding energy and inelastic reaction rates) challenging. Experimentally, the  $\psi'$  over  $J/\psi$  ratio has been measured at the SPS [10], where it was found to drop by up to a factor of 3 in central 17.3 GeV Pb-Pb collisions. This is consistent with the statistical hadronization approach [11], but it can also be explained by transport approaches with large inelastic reaction rates of the  $\psi'$  in the hadronic phase [12, 13]. More recently,  $\psi'$  data have become available for 0.2 TeV d-Au collisions at RHIC [14]

and 5.02 TeV p-Pb collisions at LHC [15].  $\psi'$  mesons were found to be significantly more suppressed than  $J/\psi$  mesons, which is difficult to reconcile with initial cold-nuclear-matter (CNM) effects since the passing time of the highly Lorentz-contracted incoming nuclei is much smaller than the formation time scale of the charmonia. Consequently, final-state effects have been put forward to explain these data, e.g., using the comover suppression model [16], which achieves a good description of the collision energy and rapidity dependence of the  $\psi'$  and  $J/\psi$  including the expected CNM effects on the parton distribution functions (see also Ref. [17]).

However, rather unexpected results have emerged from recent measurements by the CMS collaboration [18] for the double-ratio of the nuclear modification factor,  $R_{AA}$ , of  $\psi'$  over  $J/\psi$  in 2.76 TeV Pb-Pb collisions at the LHC (preliminary results are also available from ALICE [19]). At slightly forward rapidities,  $1.6 < |y| < 2.4$ , and for transverse momenta  $3 < p_t < 30$  GeV, this double ratio is around  $0.9 \pm 0.45 \pm 0.3$  for peripheral and semi-central collisions, but significantly exceeds one for central collisions,  $2.3 \pm 0.5 \pm 0.35$ . Especially the latter has evaded any model explanations thus far, see, e.g., the detailed studies in Ref. [20]. On the other hand, around midrapidity, and for momenta  $6.5 < p_t < 30$  GeV, a double ratio of around  $\sim 0.5$  is found, which is much more in line with common expectations of a stronger suppression of  $\psi'$  due to its much weaker binding.

In the present paper we put forward a potential mechanism to (partially) resolve the above “puzzle”. Based on the rather large inelastic reaction rates for the  $\psi'$  in hadronic matter that we deduce from its suppression in d-Au (also in line with the aforementioned SPS data), we argue that the inverse reactions of  $\psi'$  formation in Pb-Pb collisions must also happen in the later, hadronic stages of the fireball evolution. In particular, the  $\psi'$  regeneration processes happen later than those for the  $J/\psi$  whose

much larger binding energy leads to an earlier “freezeout” than for the  $\psi'$ . The consequence of such a “sequential freezeout” is that the collective expansion velocity of the medium leads to harder  $p_t$  spectra for the  $\psi'$ , which, in terms of the  $R_{AA}$ , can outshine the  $J/\psi$  in a momentum range of  $p_t \gtrsim M_\psi$ , which happens to coincide with the CMS  $p_t$  cut. On the other hand, at higher  $p_t$ , the regeneration contribution ceases giving way to a more sequential-like suppression pattern of primordially produced charmonia.

Our paper is organized as follow: In Sec. II we update our hadronic reaction rates for both  $\psi'$  and  $J/\psi$ , apply them within a schematic fireball for d-Au collisions at RHIC and compare our results to PHENIX data. In Sec. III we implement the updated hadronic rates in our earlier constructed transport approach. In particular, we estimate for the time windows for sequential charmonium regeneration, and elaborate the uncertainty for the underlying charmonium  $p_t$  spectra in the context of the CMS data for the  $\psi'/J/\psi$   $R_{AA}$  double ratio. We conclude in Sec. IV.

## II. HADRONIC DISSOCIATION OF CHARMONIA

Dissociation rates of charmonia in hadronic matter are usually considered to be much smaller than in the QGP (see, e.g., the discussion in Ref. [2]). However, for the  $\psi'$  this is not so obvious, since the proximity of its mass to the  $D\bar{D}$  threshold provides a large phase space for break-up reactions. In the following, we revisit hadronic reactions rates for  $J/\psi$  and  $\psi'$  mesons based on effective meson Lagrangians (Sec. II A) and evaluate their consequences for final-state effects in d-Au reactions at RHIC (Sec. II B).

### A. Update on Dissociation Rates

Our starting point is the previously employed hadronic reactions rates [13] based on flavor- $SU(4)$  meson exchange models [21, 22] for the processes  $J/\psi + \rho \rightarrow D + \bar{D}, D^* + \bar{D}^*$  (exothermic for  $m_{J/\psi} + m_\rho > m_D + m_{\bar{D}}$  and endothermic for  $m_{J/\psi} + m_\rho < m_{D^*} + m_{\bar{D}^*}$ ) and  $J/\psi + \pi \rightarrow D^* + \bar{D}, D + \bar{D}^*$  (endothermic). For those reactions, the  $J/\psi$  dissociation rate at  $T=170$  MeV amounts to 1-2 MeV, corresponding to a lifetime of 100-200 fm/c. Even with the typical uncertainties (factor  $\sim 2-3$ ) associated with the hadronic formfactor cutoff values, this is too small to affect the  $J/\psi$  abundance during the 5-10 fm/c lifetime of the hadronic phase in URHICs. For the  $\psi'$ , geometric scaling by the vacuum radius has been assumed, increasing its rates by a factor  $(r_{\psi'}/r_{J/\psi})^2$ , which is approximately compatible with constituent-quark model calculations [23].

A hadron resonance gas (HRG), however, contains many more species than  $\pi$  and  $\rho$ . To estimate their

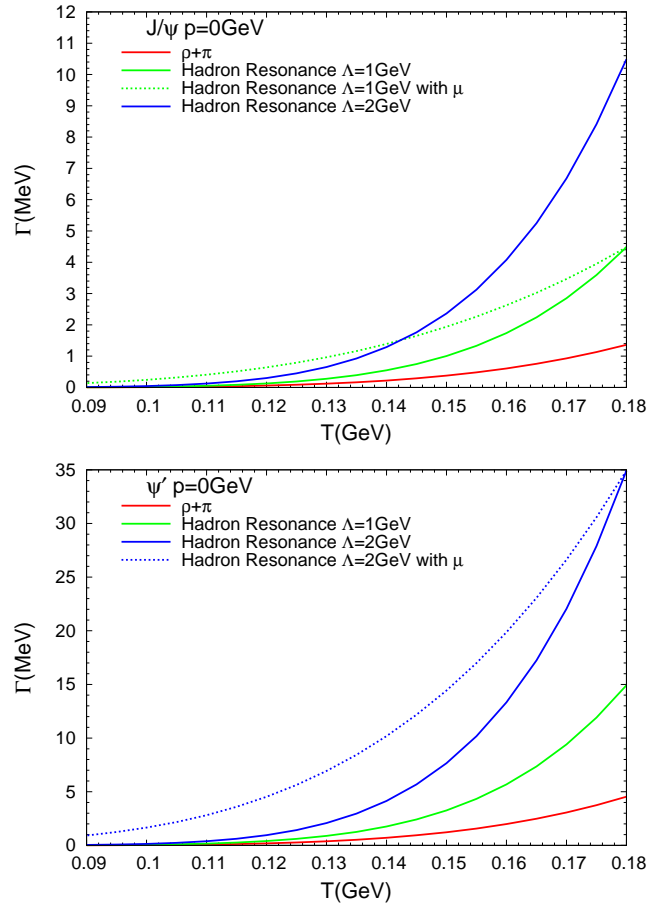


FIG. 1: (Color online) Temperature dependence of hadronic dissociation rates for  $J/\psi$  (upper panel) and  $\psi'$  (lower panel) at rest in a thermal bath. Previous results for a  $\pi\rho$  gas with  $\Lambda=1$  GeV (solid red lines) are compared to our updated results for a meson resonance gas using  $\Lambda=1$  GeV and 2 GeV (solid green and blue lines, respectively). The blue-dotted lines additionally account for finite meson chemical potential that build up for temperatures below the chemical freezeout in URHICs [24].

impact on the charmonium dissociation rates, we simply adopt the existing  $\rho$ - and  $\pi$ -induced matrix elements and shift their kinematics according to the pertinent 2-particle threshold, i.e.,

$$\Gamma_{X+J/\psi}^{\text{diss}}(T) = \int \frac{d^3k}{(2\pi)^3} f^X(E_X(k); T) \sigma_{X+J/\psi}^{\text{in}}(s, s_{\text{thr}}^X) v_{\text{rel}} \quad (1)$$

with  $s = (p_{J/\psi} + k)^2$  and  $s_{\text{thr}}^X = (m_{J/\psi} + m_X)^2$  for exothermic and  $s_{\text{thr}}^X = (2m_D)^2$  for endothermic ss ( $s_{\text{thr}}^X = (m_D + m_{D_s})^2$  if  $X$  contains a strange quark). We include a total of 52 non-strange and single-strange meson species, up to a mass of  $m_X = 2$  GeV. As before, we apply geometric scaling to obtain the reaction rates for the  $\chi_c$  and  $\psi'$ . Our results for a meson gas in chemical equilibrium are summarized by the solid lines in Fig. 1. At the highest temperature ( $T=180$  MeV), the

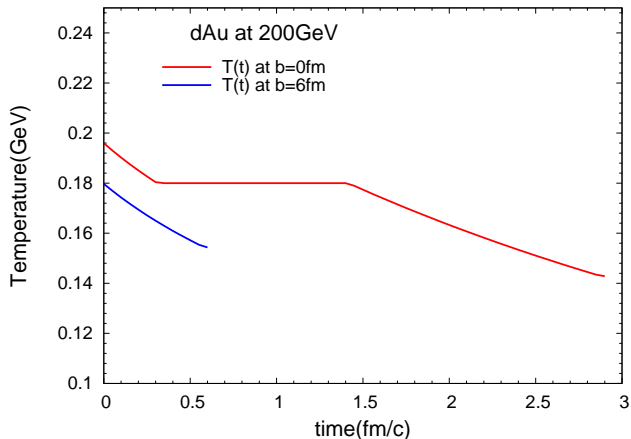


FIG. 2: (Color online) Temperature evolution in 0.2 TeV d-Au collisions assuming a thermal fireball model. The blue (red) curve is for an impact parameter of  $b=0(6)$  fm.

additional resonances enhance the  $J/\psi$  dissociation rate by factor of  $\sim 2.5$ , and another factor of 2.5 when increasing the hadronic formfactor cutoff from  $\Lambda=1$  GeV to 2 GeV, reaching a maximal rate of 10.5 MeV. For the  $\psi'$ , geometric scaling leads a maximum rate of up to 35 MeV, translating into a lifetime of 7 fm/c which is now comparable to the duration of the hadronic phase in URHICs. This becomes even more significant if chemical freezeout is accounted for, which implies the build-up of meson chemical potentials which lead to a slower decrease of the meson densities as temperature decreases, cf. dotted lines in Fig. 1.

### B. Charmonium Production in 0.2 TeV d-Au Collisions

We proceed by implementing our updated hadronic reaction rates into the thermal-rate equation framework developed in Ref. [25]. Another new aspect relative to our previous work [26] is that we allow for final-state effects in small collision systems, specifically for d-Au at RHIC, where a rather large  $\psi'$  suppression has been observed. (while  $J/\psi$ 's are much less suppressed).

Toward this end, we construct a thermal fireball using the same methods as before for AA collisions. We determine the total entropy of the fireball by matching the observed final-state hadron abundancies. Based on a Glauber model for the centrality dependent nuclear overlap function, we initialize the fireball with a transverse radius of  $R_0 \simeq 2.5$  fm/c. The expansion is then modeled with the same acceleration as in 0.2 TeV Au-Au before [26]. For simplicity, we stick with our first-order equation of state, transitioning from a quasi-particle QGP into a HRG through a mixed phase at  $T=180$  MeV (we do not expect large changes when utilizing a modern cross-over EoS, which has been checked for dilepton [27]

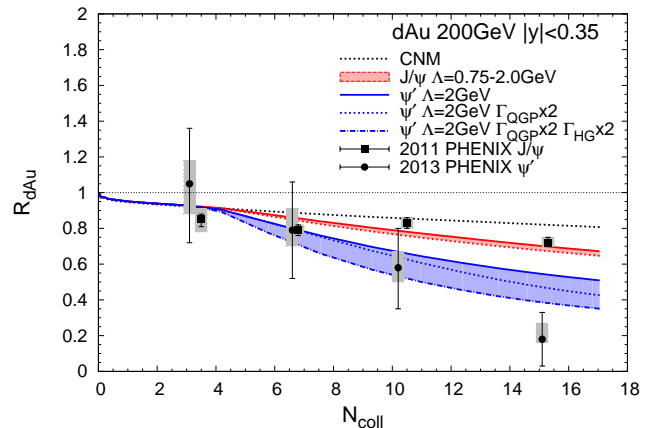


FIG. 3: (Color online) Centrality dependence of the nuclear modification factor for charmonia in 0.2 TeV d-Au collisions at RHIC; CNM effects for all charmonia are shown by the black dotted line (consistent with Ref. [16] based on the EPS09 shadowing [29] parameterization); the blue band illustrates uncertainties in both QGP and hadronic dissociation rates of the  $\psi'$ , while the red band illustrates the uncertainties due to the hadronic dissociation of the  $J/\psi$  (solid (dotted) line:  $\Lambda=0.75(2)$  GeV). The PHENIX data are from Refs. [14, 30].

and bottomonium observables [28]). Kinetic freezeout is also constructed as before, with a freezeout temperature mildly decreasing with centrality, from  $T_{fo} \simeq 155$  MeV in peripheral to  $\sim 142$  MeV in central collisions, resulting in fireball lifetimes of 0.5-3 fm we have assumed the same initial spectra for  $J/\psi$  and  $\psi'$  from pp collisions, cf. Fig. 2. For the most central collisions, a short QGP phase with initial temperature  $T_0=190$  MeV is followed by a 1 fm/c mixed phase and a 1.5 fm/c hadronic phase.

The initial CNM effects are assumed to be identical for all charmonia, essentially given by a shadowing suppression [16] which we mimic with an “effective” nuclear absorption cross section of  $\sigma_{abs}=2.4$  mb. Our results for the centrality dependence of the nuclear modification factor,

$$R_{AA}^{\Psi}(N_{part}) = \frac{N_{\Psi}(N_{part})}{N_{\Psi}^{pp} N_{coll}(N_{part})} \quad (2)$$

are summarized for both  $\Psi = J/\psi, \psi'$  in Fig. 3, in comparison to PHENIX data [14] ( $N_{coll}$ : number of primordial  $NN$  collisions). For the  $J/\psi$ , there is little suppression beyond CNM effects; the additional final-state effects are due to a small QGP suppression on the direct  $J/\psi$ 's, as well as a suppression of the feeddown from  $\chi_c$ 's and  $\psi'$ , with little room for additional hadronic suppression (thus, in principle, preferring a small value for the hadronic cutoff parameter). On the other hand, for the  $\psi'$ , our baseline QGP suppression is not enough to account for the marked suppression beyond CNM effects. Here, a large formfactor cutoff of  $\Lambda=2$  GeV is preferred to augment the hadronic suppression. An additional increase of QGP suppression rate of the  $\psi'$  by a factor of

2 could also be helpful (such an increase may arise, e.g., from nonperturbative heavy-quark interactions with light partons). Further increasing the hadronic rate by a factor of  $2^1$  goes in a similar direction, i.e., reducing the discrepancy with the most central data point.

We finally note that a hadronic  $\psi'$  dissociation rate well beyond the one from the  $\pi\rho$  gas (by a factor of 5 or more) was previously deduced within our setup [13] to be able to account for the  $\psi'$  suppression observed in S-U and Pb-Pb collisions at the SPS [10]. Our newly calculated rates in the present ms. are in line with this notion.

### III. SEQUENTIAL REGENERATION OF CHARMONIA

In this section, we investigate the consequences of the updated hadronic reaction rates within our previously constructed thermal fireball expansion (Sec. III A), followed by a more generic evaluation of the associated uncertainties specifically in the context of the  $\psi'/J/\psi$   $R_{AA}$  double ratio (Sec. III B). We focus on 2.76 TeV Pb-Pb collisions at the LHC. Our earlier predictions for inclusive  $J/\psi$  production in these reactions [5] resulted in a fair agreement with the centrality, transverse-momentum and rapidity dependencies observed by the ALICE and CMS collaborations, and thus serves as our framework to evaluate  $\psi'$  observables. Since the pertinent CMS data are for “prompt”  $J/\psi$  and  $\psi'$  production, we do not include contributions from  $B$  feeddown.

#### A. Fireball Model

For our fireball results we focus on the so-called “strong-binding scenario”, where the in-medium charmonium properties are taken with guidance from a  $T$ -matrix approach with the internal energy from lattice-QCD as underlying potential. This assumption gives a better agreement both with correlators from lattice-QCD [31] and the overall charmonium phenomenology at SPS and RHIC [26]. For definiteness, we employ the hadronic rates with  $\Lambda=0.75(2)$  GeV for the  $J/\psi$  ( $\psi'$ ), and the factor-of-2 increased QGP rate of the  $\psi'$ .

Let us first inspect the time evolution of direct  $J/\psi$  and  $\psi'$  mesons in 0-20% central Pb-Pb at midrapidity (without shadowing), as following from the solution of the kinetic rate equation,

$$\frac{dN_{\Psi}}{d\tau} = -\Gamma_{\Psi}(N_{\Psi}(\tau) - N_{\Psi}^{\text{eq}}(T(\tau))), \quad (3)$$

<sup>1</sup> This could be due to inelastic reactions with baryons and antibaryons or direct  $\psi' \rightarrow D\bar{D}$  decays with an in-medium reduced  $D$  meson mass [25], neither of which we have calculated here.

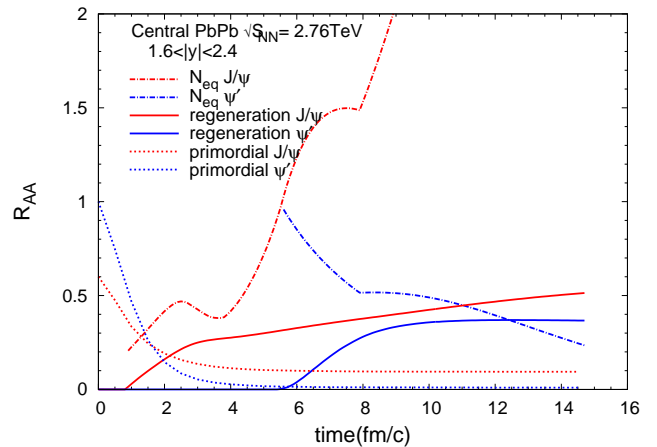


FIG. 4: (Color online) Time dependence of  $J/\psi$  and  $\psi'$  nuclear modification factors in central ( $N_{\text{part}}=324$ ) Pb-Pb collisions at  $\sqrt{s}=2.76$  TeV (the denominator for the  $J/\psi$   $R_{AA}$  includes 40% feeddown from excited states while the numerator does not). The red (blue) curves are for direct  $J/\psi$  ( $\psi'$ ), with the solid (dotted) line styles representing the regeneration (primordial) contributions; the dash-dotted curves indicate the pertinent equilibrium limits (including a thermal relaxation time correction [13]), starting from the time when the fireball has cooled down to the dissociation temperature below which regeneration commences.

see Fig. 4. Compared to our previous results (cf. lower panel in Fig. 2 of Ref. [5]), the  $J/\psi$  now picks up a regeneration contribution in the hadronic phase, by about 0.15 units in  $R_{AA}$ , which, despite a small rate, is due to the large equilibrium limit. Most of the production, however, occurs prior to the onset of the mixed phase at  $\tau \simeq 5.5$  fm/c. On the contrary,  $\psi'$  production only starts to set in at that point, leveling off around  $\tau \simeq 9-10$  fm/c, when the temperature of the fireball has dropped to about 150-160 MeV. The main qualitative and robust feature here is that the lower dissociation temperature of the  $\psi'$ , relative to the  $J/\psi$ , implies a later production through regeneration in the time evolution of the fireball in URHICs.

The sequential regeneration of  $J/\psi$  and  $\psi'$  has rather dramatic consequences on their transverse-momentum ( $p_t$ ) spectra. Following our previous work [32], we approximate the  $p_t$  spectra of the regeneration components with the standard blast-wave expression,

$$\frac{dN_{\Psi}^{\text{reg}}}{p_t dp_t} = N_0(b) m_t \int_0^R r dr K_1\left(\frac{m_t \cosh \rho(r)}{T}\right) I_0\left(\frac{p_t \sinh \rho(r)}{T}\right) \quad (4)$$

implying thermalized charm-quark distributions. As our default, we evaluate this expression when most of the pertinent charmonium yield has built up, i.e., at  $T_c$  for the  $J/\psi$  ( $\tau=5.5$  fm/c in Fig. 4) and at  $T=155$  MeV for the  $\psi'$  ( $\tau=9.7$  fm/c in Fig. 4). The resulting nuclear modification factors for both regeneration and surviving primordial components are displayed in Fig. 5 (we have assumed the same initial spectra for  $J/\psi$  and  $\psi'$  from  $pp$  collisions,

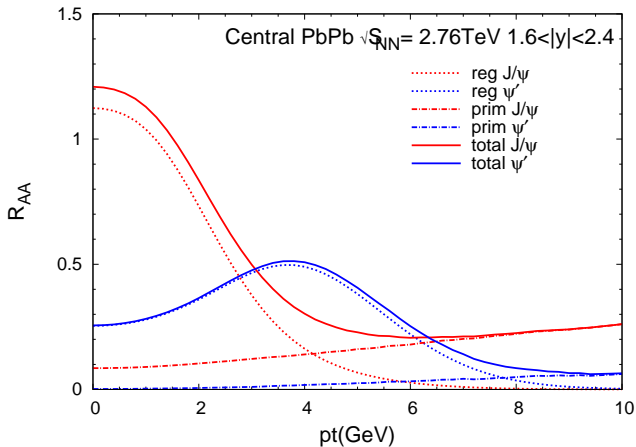


FIG. 5: (Color online) Nuclear modification factor for  $J/\psi$  (red lines) and  $\psi'$  mesons (blue lines) as a function of  $p_t$  for 0-20% Pb-Pb(2.76 TeV) collisions. The total  $R_{AA}$  for each meson (solid lines) is decomposed in a regeneration component (dotted lines, evaluated with a blast-wave ansatz in the fireball evolution at sequential freezeout times) and a suppressed primordial component (dash-dotted lines, as obtained from a Boltzmann transport equation without gain term), cf. Ref. [32] for further details.

figuring into the denominator of  $R_{AA}$ ). Clearly, there is a significant uncertainty associated with this procedure which we address in Sec. III B below (we recall, however, that our pertinent predictions for the  $J/\psi$  gave fair agreement with the observed  $p_t$  spectra at LHC). Three main qualitative features can be gleaned from comparing the  $R_{AA}$ 's for  $J/\psi$  and  $\psi'$  in Fig. 5: (a) At low  $p_t \lesssim 3$  GeV, the regeneration yield of the  $J/\psi$  dominates over the one from  $\psi'$ , as a consequence of the approach toward equilibrium which favors the smaller  $J/\psi$  mass; (b) At “intermediate”  $p_t \simeq 3 - 6$  GeV, the significantly harder blast wave for the  $\psi'$  generates a shift of the “flow bump” which can exceed the regeneration contribution in the  $J/\psi$   $R_{AA}$ ; (c) at still higher momenta,  $p_t \gtrsim 6 - 8$  GeV, regeneration gives way to (suppressed) primordial production, where the  $J/\psi$   $R_{AA}$  exceeds again the one from the more weakly bound  $\psi'$ . Items (b) and (c) are in qualitative agreement with the trends observed in the pertinent  $R_{AA}^{\psi'}/R_{AA}^{J/\psi}$  double ratio observed by CMS [18]. In the next section we explore some of the uncertainties in our calculations.

## B. Schematic Model

To better quantify variations in the interplay of the different production components of both  $J/\psi$  and  $\psi'$ , let us first formulate a baseline scenario motivated by existing experimental data for the  $J/\psi$  and the thermal fireball calculations in the previous sections. For simplicity, we assume the primordial parts to be constant in  $R_{AA}(p_t)$ . For 0-20% Pb-Pb collision we take 0.15-0.25 for the  $J/\psi$  (compatible with high- $p_t$  CMS data

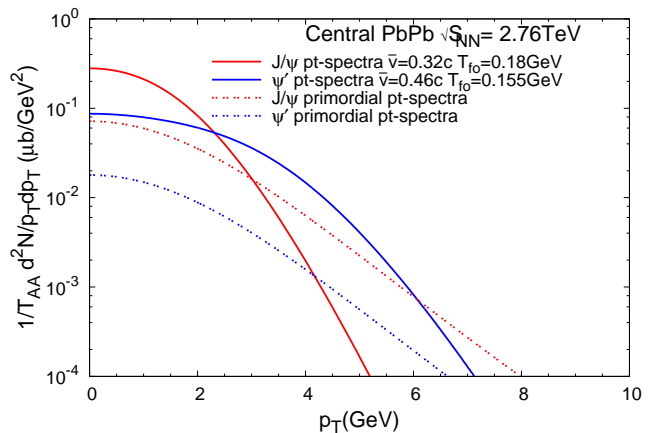


FIG. 6: (Color online) Transverse-momentum spectra of  $J/\psi$  (red lines) and  $\psi'$  mesons (blue lines) for both suppressed primordial (dashed lines, assuming  $R_{AA}^{J/\psi}=0.2$  and  $R_{AA}^{\psi'}=0.05$ ) and regeneration components (solid lines); the total yields (not the shapes) are normalized to their  $N_{\text{coll}}$ -scaled number in  $pp$  collisions.

for prompt  $J/\psi$  [33]) and 0-0.075 for the  $\psi'$ , to reflect its stronger absorption as a loosely bound states. The constancy in  $p_t$  reflects our currently limited knowledge about the  $p_t$  dependence of the dissociation rates (see, e.g., Ref. [32]), formation time effects, etc. For the regeneration components, we choose total yields such that the total momentum-integrated  $R_{AA}$  amounts to 0.55-0.65 for the  $J/\psi$  (compatible with ALICE data [34]) and 0.4 for the  $\psi'$  (as suggested by our fireball results). For the sequential freezeout, which determines the temperature and flow strength in the blast-wave spectra of the regeneration components, we stick with the correlation given by the expanding fireball, i.e.,  $\tau \simeq 5.5(9.7)$  fm/c for the  $J/\psi$  ( $\psi'$ ) corresponding to  $T_{fo}=180(155)$  MeV and  $\bar{v}=0.32(0.46)c$ . Recall that the effective slope parameter for the blast-wave spectra is approximately given by  $T_{\text{eff}} \approx T + m_{\psi} \bar{v}^2$ , which is mostly driven by the flow term due to the large mass of the charmonia. In Fig. 6 we display the pertinent  $p_t$  spectra for central Pb-Pb(2.76 TeV), normalized by the  $N_{\text{coll}}$ -scaled yields in  $pp$ , to mimic the relative magnitude of  $\psi'$  and  $J/\psi$  contributions in their respective  $R_{AA}$ 's. The plot highlights again the main effect proposed in this paper: due to the stronger flow for the regenerated  $\psi'$ , its  $R_{AA}$  can rise above the one for the  $J/\psi$  in a limited  $p_t$  window around 3-6 GeV, before primordial production takes over again.

For semi-central Pb-Pb (20-40%) we construct the baseline following the same reasoning as for central collisions. We increase the primordial  $R_{AA}$ 's for  $J/\psi$  to 0.35-0.45 [33] and to 0.1-0.2 for  $\psi'$ , and evaluate the blast-wave  $p_t$  spectra at the same freezeout temperatures as for central collisions (but with flow velocities given by the fireball expansion for 20-40% centrality).

The resulting double ratios covering the above-specified ranges in the primordial components are shown

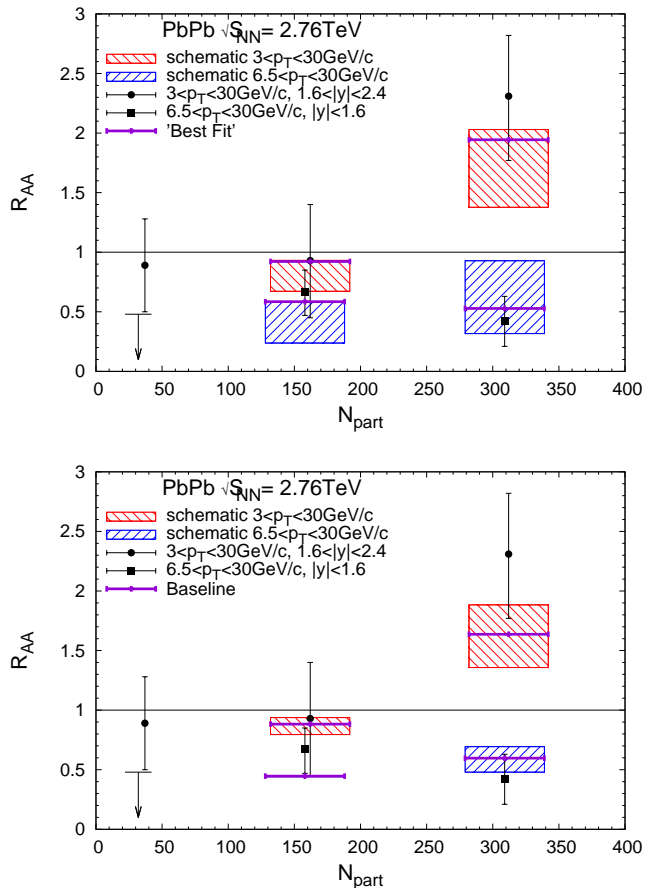


FIG. 7: (Color online) Ratio of the  $R_{AA}$  for  $\psi'$  to the one for  $J/\psi$  (the so-called “double ratio”) as a function of centrality in 2.76 TeV Pb-Pb collisions. The red and blue boxes are our schematic-model results for the double ratio in the momentum range  $p_t=3-30$  GeV and  $p_t=6.5-30$  GeV, respectively, and are compared to CMS data [18]. In the upper (lower) panel, the boxes indicate theoretical uncertainties in the modeling of the primordial (regeneration) component of the charmonium yields and spectra. The vertical purple lines represent our “best fit” in the upper panel, and a “realistic” baseline for the blast-wave variations in the lower panel.

in the upper panel of Fig. 7 and compared to CMS data [18] (we did not include the ALICE data [19] as they contain feeddown contributions from  $B$ -meson decays, which could become rather significant at high  $p_t$ , see, e.g., Ref. [20] for a calculation including those). The basic trends of the data can be reproduced within our approach. For definiteness, we quote (approximate) “best fit” value of 0.15 and  $\sim 0$  (0.35 and 0.2) for the primordial  $J/\psi$  and  $\psi'$  values, respectively, in (semi-) central Pb-Pb collisions, resulting in the purple horizontal bars in the upper panels of Fig. 7.

Finally, we illustrate the sensitivity of the double ratios to the blast-wave parameters, by varying the freezeout

temperatures over the ranges  $T_{fo}^{J/\psi}=180-200$  MeV and  $T_{fo}^{\psi'}=150-165$  MeV, along with the pertinent flow velocities from the fireball model, and fixing the primordial components at  $R_{AA}^{J/\psi}=0.2(0.35)$  and  $R_{AA}^{\psi'}=0.05(0.15)$  for (semi-) central Pb-Pb. The larger regeneration components and larger flow velocities in central collisions render the double ratios more sensitive to the details of the sequential regeneration mechanism.

#### IV. CONCLUSIONS

In the present work, we have investigated the production systematics of  $\psi'$  mesons in URHICs. We first revisited the problem of hadronic  $\psi'$  dissociation and found that a more complete inclusion of hadronic states in a resonance gas suggests a marked increase of its inelastic reaction rates. When implementing these rates into an expanding fireball for d-Au collisions at RHIC, we found a much improved description of the rather strong suppression of  $\psi'$  mesons observed in these reactions. This is similar in spirit to, and thus supports, the recently suggested comover suppression effects [16] in dA and pA reactions at RHIC and LHC. We then evaluated  $\psi'$  transport in Pb-Pb collisions at the LHC using our existing fireball approach which previously provided fair agreement with  $J/\psi$  data. The key features in our approach are the lower dissociation temperature of the  $\psi'$  relative to the  $J/\psi$  and its sizable hadronic reaction rates. This implies a sequential freezeout of those two mesons, with most of the  $\psi'$  regeneration occurring later in the fireball evolution. The larger collective medium flow then leads to a marked enhancement of the  $\psi'$  regeneration yield in a  $p_t$  region around 3-6 GeV, transitioning to (suppressed) primordial production at higher  $p_t$ . While quantitative predictions of this mechanism are beyond current theoretical control, we have shown that variations in the ingredients to the sequential regeneration scenario produce trends in the  $\psi'$  over  $J/\psi$   $R_{AA}$  double ratio which agree with recent CMS data. We therefore believe that the qualitative features of this mechanism are robust and provide a promising candidate to contribute to the understanding of these data. In fact, if corroborated, sequential regeneration may serve as a tool to extract in-medium properties of the  $\psi'$  from URHIC data.

#### Acknowledgments

We are indebted to Xingbo Zhao for providing us with his codes and valuable discussions. This work is supported by the US National Science Foundation under grant no. PHY-1306359.

- 
- [1] T. Matsui and H. Satz, Phys.Lett. **B178**, 416 (1986).
- [2] R. Rapp, D. Blaschke, and P. Crochet, Prog. Part. Nucl. Phys. **65**, 209 (2010).
- [3] L. Kluberg and H. Satz (2009).
- [4] P. Braun-Munzinger and J. Stachel, Landolt-Bornstein **23**, 424 (2010).
- [5] X. Zhao and R. Rapp, Nucl. Phys. **A859**, 114 (2011).
- [6] K. Zhou, N. Xu, Z. Xu, and P. Zhuang, Phys.Rev. **C89**, 054911 (2014).
- [7] T. Song, K. C. Han, and C. M. Ko, Phys.Rev. **C84**, 034907 (2011).
- [8] E. Ferreira, Phys.Lett. **B731**, 57 (2014), 1210.3209.
- [9] A. Andronic, P. Braun-Munzinger, K. Redlich, and J. Stachel, J.Phys. **G37**, 094014 (2010).
- [10] M. Abreu et al. (NA50), Nucl.Phys. **A638**, 261 (1998).
- [11] P. Braun-Munzinger and J. Stachel, Phys. Lett. **B490**, 196 (2000).
- [12] H. Sorge, E. V. Shuryak, and I. Zahed, Phys.Rev.Lett. **79**, 2775 (1997).
- [13] L. Grandchamp and R. Rapp, Nucl. Phys. **A709**, 415 (2002).
- [14] A. Adare et al. (PHENIX), Phys.Rev.Lett. **111**, 202301 (2013).
- [15] B. B. Abelev et al. (ALICE), JHEP **1412**, 073 (2014), 1405.3796.
- [16] E. Ferreira (2014), 1411.0549.
- [17] Y. Liu, C. M. Ko, and T. Song, Phys.Lett. **B728**, 437 (2014).
- [18] V. Khachatryan et al. (CMS), Phys. Rev. Lett. **113**, 262301 (2014).
- [19] R. Arnaldi (ALICE), Nucl.Phys. **A904-905**, 595c (2013).
- [20] B. Chen, Y. Liu, K. Zhou, and P. Zhuang, Phys.Lett. **B726**, 725 (2013).
- [21] Z.-w. Lin and C. Ko, Phys. Rev. **C62**, 034903 (2000).
- [22] K. L. Haglin and C. Gale, Phys. Rev. **C63**, 065201 (2001).
- [23] T. Barnes, E. Swanson, C. Wong, and X. Xu, Phys. Rev. **C68**, 014903 (2003).
- [24] R. Rapp, Phys. Rev. **C66**, 017901 (2002).
- [25] L. Grandchamp, R. Rapp, and G. E. Brown, Phys. Rev. Lett. **92**, 212301 (2004).
- [26] X. Zhao and R. Rapp, Phys. Rev. **C82**, 064905 (2010).
- [27] R. Rapp, Adv. High Energy Phys. **2013**, 148253 (2013).
- [28] A. Emerick, X. Zhao, and R. Rapp, Eur. Phys. J. **A48**, 72 (2012).
- [29] K. Eskola, H. Paukkunen, and C. Salgado, JHEP **0904**, 065 (2009).
- [30] A. Adare et al. (PHENIX), Phys.Rev.Lett. **107**, 142301 (2011).
- [31] F. Riek and R. Rapp, Phys. Rev. **C82**, 035201 (2010).
- [32] X. Zhao and R. Rapp, Phys. Lett. **B664**, 253 (2008).
- [33] S. Chatrchyan et al. (CMS), JHEP **1205**, 063 (2012).
- [34] B. B. Abelev et al. (ALICE), Phys. Lett. **B734**, 314 (2014).